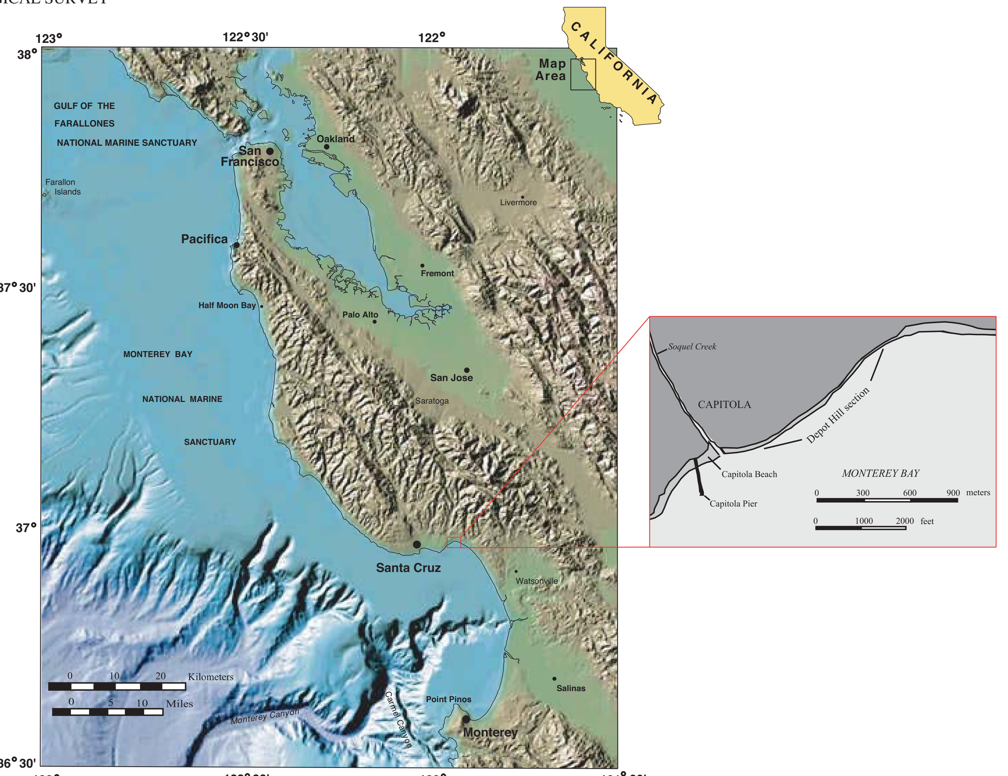

Modified from Maher and Wong, 2001

Figure 1. Location map.

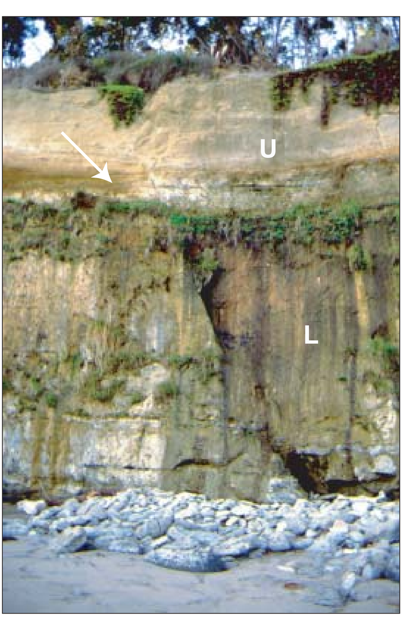

Figure 2. Photograph showing typical exposure of Purisima Formation along the Depot Hill. Note the light colored upper unit (U) and the dark lower unit (L), as well as seepage at the contact with vegetation (see arrow). Terrace deposits are not present in this photograph due to erosion.

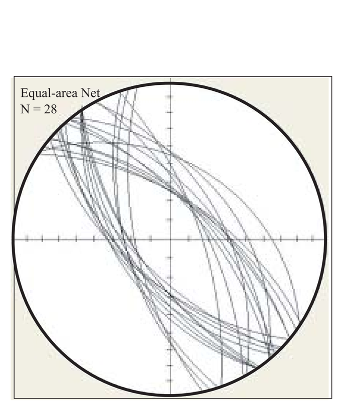

Figure 5. Stereonet plot of fault planes along Depot Hill. Faults with the same orientation plot on top of each other.

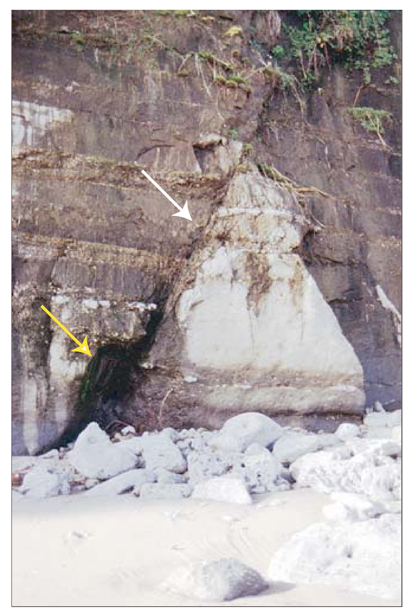

Figure 3. Photograph showing west-dipping normal fault along Depot Hill. White arrow shows fault plane, and yellow arrow shows cave where fault intersects beach.

INTRODUCTION

The coastal cliffs along much of the central California coast are actively retreating. Large storms and periodic earthquakes are responsible for most of the documented seacliff slope failures. Long-term average erosion rates calculated for this section of coast (Moore and others, 1999) do not provide the spatial or temporal data resolution necessary to identify the processes responsible for retreat of the seacliffs, where episodic retreat threatens homes and community infrastructure. Research suggests that more erosion occurs along the California coast over a short time scale, during periods of severe storms or seismic activity, than occurs during decades of normal weather or seismic quiescence (Griggs and Scholar, 1998; Griggs, 1994; Plant and Griggs, 1990; Griggs and Johnson, 1979 and 1983; Kuhn and Shepard, 1979).

This is the first map in a series of maps documenting the processes of short-term seacliff retreat through the identification of slope failure styles, spatial variability of failures, and temporal variation in retreat amounts in an area that has been identified as an erosion hotspot (Moore and others, 1999; Griggs and Savoy, 1985). This map presents seacliff failure and retreat data from Depot Hill, California, which is located five kilometers east of Santa Cruz (fig.1) near the town of Capitola, along the northern Monterey Bay coast. The data presented in this map series provide high-resolution spatial and temporal information on the location, amount, and processes of seacliff retreat in Santa Cruz, California. These data show the response of the seacliffs to both large magnitude earthquakes and severe climatic events such as El NiÒos; this information may prove useful in predicting the future response of the cliffs to events of similar magnitude. The map data can also be incorporated into Global Information System (GIS) for use by researchers and community planners.

Four sets of vertical aerial photographs (Oct. 18, 1989; Jan. 27, 1998; Feb. 9, 1998; and March 6, 1998) were orthorectified and digital terrain models (DTMs) were generated and edited for this study (see Hapke and Richmond, 2000, for description of techniques). The earliest set of photography is from 1989, taken immediately following the Loma Prieta earthquake. These photographs are used to document the response of the seacliffs to seismic shaking, as well as to establish an initial cliff-edge position to measure the amount of retreat of the cliff edge over the following decade. The remaining three sets of photographs were collected using the U.S. Geological Survey Coastal Aerial Mapping System (CAMS) during the 1997-98 El NiÒo (see Hapke and Richmond, 1999, 2000). The CAMS photographs were taken before, during, and after severe storms and are used to examine seacliff response to these storms. In addition to the analyses of photogrammetrically processed data, field mapping identified joints, faults, and lithologic variations along this section of seacliff.

GEOLOGY

The one-kilometer-long stretch of Depot Hill is characterized by high, near-vertical cliffs backing a narrow beach. The 18- to 32-m-high cliffs are composed of the Miocene to Pliocene Purisima Formation, which is capped by a 4- to 6-m-thick layer of unconsolidated Pleistocene terrace deposits (Dupre, 1975; Greene, 1977; Brabb, 1989). The Purisima Formation consists of massively bedded siltstones and sandstones that contain interbedded layers of shell-hash deposits. In this exposure, the Purisima Formation is highly jointed and faulted and is characterized by two distinct stratigraphic units (figs. 2, 3, and 4): an upper, less lithified, more permeable unit (the sandstone member of Plant and Griggs, 1990) and a lower, more indurated unit (the siltstone member of Plant and Griggs, 1990) that acts as an aquitard except where it is fractured. Water seeps are common year round at the contact between these two units (fig. 2). The Purisima Formation dips gently eastward (4-5∞) in this area; as a result of this dip and larger throws on the down-to-the-east normal faults, the sandstone member is not exposed above the beach level in the easternmost portion of Depot Hill (fig. 4). Here, the entire 28-m-high cliff is composed of the siltstone member of the Purisima Formation and 4 to 6 m of terrace deposits. Figure 5 shows an equal-area stereonet plot of the 28 faults (only 25 faults are visible in figure 4 because three of the faults have the same strike and dip of others and thus the plots fall on top of each other) that were mapped along this section of coast. The general geology, including some of the faults, is represented schematically in the cross-section (fig. 4). Note that all the faults strike northwest (average azimuth is 320∞), and the average dip is 67∞.

A narrow beach that is completely flooded at high tide lies in front of the cliffs along Depot Hill. Therefore, the base of the cliff is subjected daily to marine hydraulic and abrasive scouring. This results in undercutting which is accelerated in areas where faults intersect the beach (fig. 4). Differential retreat occurs as a result of facies variation and structural weaknesses exposed at water level. This differential retreat is reflected in the cliff morphology by numerous embayments and reentrants at a scale of tens of meters. This morphologic variation is shown in the orthophotomosaic (fig. 6).

WAVE AND CLIMATIC SETTING

The wave climate is well documented for the northern Monterey Bay (U.S. Army Corps of Engineers, 1985). Existing data from wave-gage records and wave hindcasts show that deep water waves have a mean height of 1.2 m and a mean period of 13 seconds. The waves most frequently arrive from the northwest, but they do approach from due south through north-northwest. During El NiÒo winters, storm waves arrive more frequently from the west and southwest than during non-El NiÒo winters, and heights of three meters or greater are more common during El NiÒo years than non-El NiÒo years. Wave refraction studies (U.S. Army Corps of Engineers, 1985) show that for the portion of coastline of northern Monterey Bay that includes Depot Hill, waves approaching from the northwest diverge significantly around Point Santa Cruz at the northwestern entrance to the Monterey Bay, changing nearly 100∞ to approach the shore from the southwest. Wave height (and consequently wave energy) is thus reduced before reaching the shoreline. However, waves approaching from the southwest undergo less refraction because there is no headland to dissipate wave energy. As a result, waves from the southwest have greater heights and more energy upon reaching the shoreline. The highest waves reaching the shoreline in northern Monterey Bay are commonly storm waves approaching from the southwest to west.

Tides in this region are diurnal and have a mean range of 1.6 m; the highest high water is 2.4 m and the lowest low is -0.8 m (U.S. Army Corps of Engineers, 1985). The highest monthly tides occur in the winter and summer; it is not unusual for the highest tides to coincide with large, winter storm waves.

Rainfall in this region occurs predominantly from December through March, and high rainfall frequently coincides with large waves. The average annual precipitation since 1895 is 53 cm, although large climatic perturbations such as El NiÒo can bring excessive precipitation to the area. Based on data compiled by Storlazzi and Griggs (2000), 76 percent of historical storms that caused significant coastal erosion or damage occurred during El NiÒo years.

SEISMIC AND CLIMATIC EVENTS

This study documents the impacts of earthquakes and large storms to the seacliffs of Depot Hill. The first event is the 1989 Loma Prieta earthquake, a 7.1 magnitude earthquake that caused widespread damage to the area stretching from Santa Cruz to the San Francisco Bay. The epicenter of the earthquake was located in the Santa Cruz Mountains, approximately 9 km inland from the coast. Peak accelerations in the vicinity of the coastal cliffs were estimated to be on the order of 0.47 g to 0.64 g (horizontal) and 0.40 g to 0.66 g vertical (Sydnor and others, 1990). Extensive block and debris falls, induced by the seismic shaking, occurred along the seacliffs in the study area (Plant and Griggs, 1990; Sydnor and others, 1990). Plant and Griggs (1990) describe the seacliff failures in detail; in addition to the slope failures, they also describe tension cracks that developed parallel to and landward of the cliff face. These cracks may be important in determining locations of failures in the days, weeks, and even years following the earthquake by providing failure planes and zones along which groundwater flow may be focused.

The second major event considered in this study is the 1997-98 El NiÒo that brought increased winter storm activity to the coastline of the northern Monterey Bay. Associated with these storms, which began in force in late January of 1998, were increased wave energy from westerly directions, elevated sea level, and increased amount and duration of precipitation. While increased wave energy and elevated sea level potentially have significant impacts on those portions of the cliffs that are exposed to waves, increased rainfall leading to excessive surface wash and increased groundwater pore pressures also promote erosion of the seacliffs.

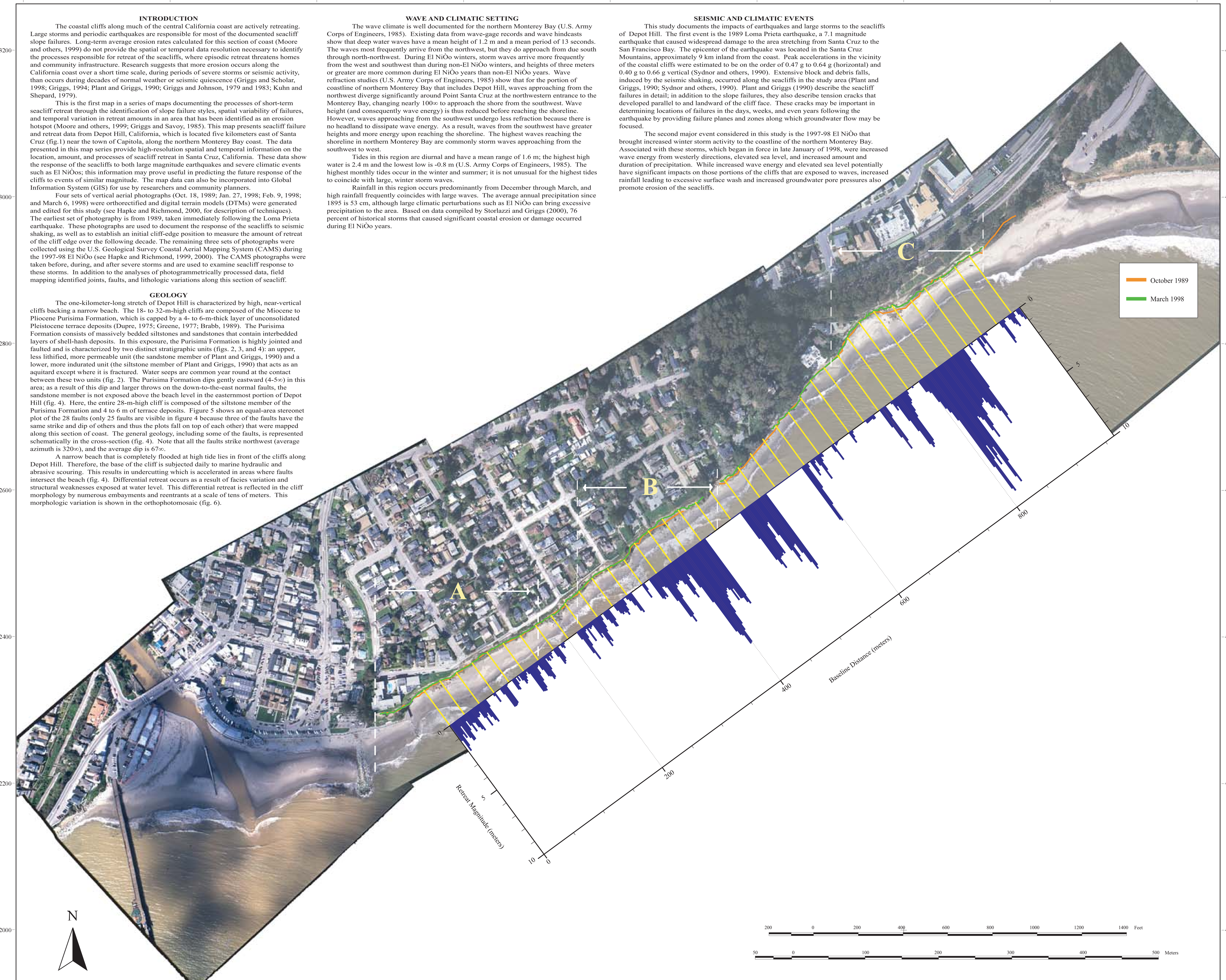

Aerial photograph from Coastal Aerial Mapping System (CAMS), March 6, 1998

Universal Transverse Mercator projection, zone 10

Figure 6. Orthophotomosaic (from CAMS imagery flown 3/6/98 at a scale of 1:7500) of Depot Hill showing retreat magnitude and cliff edge positions. Note that the baseline is shorter than the along-cliff distance (fig.9) because the baseline is a straight line approximating the average trend of this section of coast and figure 9 is showing the actual along-cliff distance.

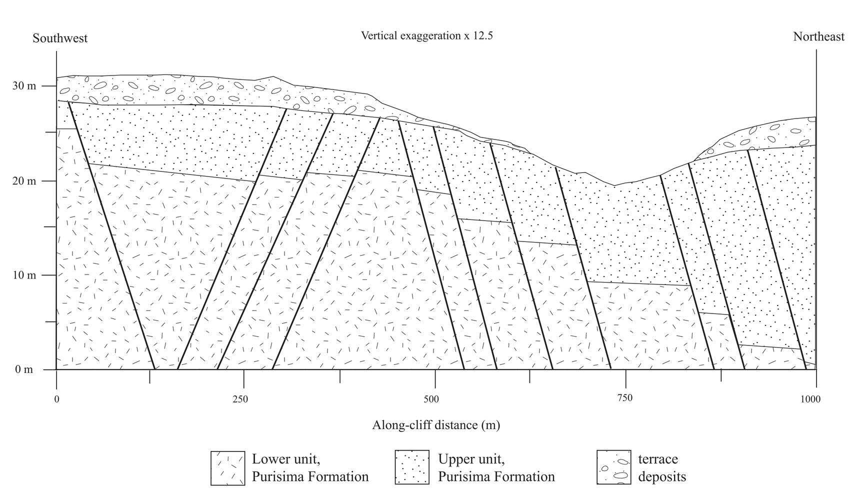

Figure 4. Schematic cross section of Depot Hill. A total of 28 faults were mapped along this section of coast; no attempt is made to show them all here. Instead, this cross section shows the general trends: conjugate normal faults with larger magnitude offsets along the down-to-the-east faults. This results in a pinching out of the lower unit of the Purisima Formation at the east end of the section.

CLIFF RETREAT

The amount of cliff retreat for Depot Hill was determined by digitizing the top edge of the cliff on the rectified photographic stereo models from October 1989 and from March 1998. Digitizing while viewing in stereo ensures that the true topographic break in the terrain is used as the cliff edge. The cliff edge is typically sharp and easy to identify, but in some areas it is completely obscured by large trees or other vegetation. The amount of landward retreat of the cliff edge was measured as the difference in distance between two cliff edges (as digitized on the October 1989 and March 1998 stereomodels) as measured from a shore parallel baseline. The use of shore parallel baselines in measuring coastal change is a common technique in coastal studies (Anders and Burns, 1991; Thieler and Danforth, 1994). For this map, the positional accuracy is less than one meter, based on the scale of the photography, the scan resolution, and global positioning system (GPS) survey data used in the orthorectification process.

The orthophotomosaic in figure 6 shows the cumulative seacliff retreat and morphologic evolution of this stretch of coast from October 1989 to March 1998. The October 1989 data (orange line) shows the position of the upper cliff edge immediately following the magnitude 7.1 Loma Prieta earthquake, and the March 1998 data (green line) represents the position of the cliff edge following the last of the severe 1997-98 El NiÒo storms. The amount of retreat in the bar graph in figure 6 shows a maximum retreat of 9.1 m; the average retreat along this section of coast is 2.1 m. The baseline from which the cliff edge positions are measured for retreat calculations is parallel to the average trend of this section of cliffs. However, the cliff morphology is highly crenulated and as a result the length of the baseline (fig. 6) is shorter than the actual along-cliff distance.

The maximum cliff retreat, located near the eastern end of the section, is a large blockfall; the deposit is visible on the beach on figure 6. The western 300 m of the section appear to be more stable; retreat amounts of 2 m or less are more common than in the central and eastern part of the section where localized retreat amounts of 7 to 9 m occur approximately every 100-200 m.

The amount that a particular section of cliff retreats in a given time period provides quantitative information that may be useful to land-use planning and land owners. While such retreat information is valuable, it provides little information on the processes of slope failure that lead to seacliff retreat.

PROCESSES OF SEACLIFF FAILURE

During this study we developed a method for investigating short-term processes of seacliff evolution using rectified photographic stereo models. This method allows us to document the linear extent of cliff failures, the spatial and temporal relationship between failures, and the type or style of slope failure.

In order to document the along-cliff linear extent of slope failure associated with a particular period or event, first the top edge of the cliff was digitized from the rectified photographic stereo model at high resolution (0.2 m/pixel) for each date of photography. At each location where slope failure was observed, either by retreat of the cliff edge or by visible deposits at the base of the cliff, the position, linear extent and characteristics of the cliff failure were documented. The characteristics for each occurrence of slope failure include the amount of retreat, if any, the type of failure (debris fall, block fall, debris flow), physical descriptions such as the shape of the scar (linear or cuspate), and the geologic unit involved. The type of cliff failure was determined by both the nature of the failure scar and the deposit on the beach below and is based on classifications and descriptions by Varnes (1958). The linear extent of places where the cliff has failed is demarcated for each date of photography by overlaying the representation of the cliff edge that was digitized from the previous date of photography on the current rectified photographic stereo model (for example Oct. 1989 digitized cliff edge positioned over Jan. 1998 stereo model) and delineating the places where visible slope failure or retreat of the top edge of the cliff have occurred during the period between the two dates of photography. For each linear extent of slope failure the location and characteristics of each individual failure for each date are recorded. An important finding of this study is that slope failures do not always result in retreat of the cliff edge. Failures can occur on the seaward face of the cliff where there is no actual landward retreat of the top edge of the cliff. These slope failures are identified by the existence of fresh scars and deposits that are visible in the photographic stereo models. The cliff failures that do not result in measurable retreat of the top edge of the cliff may result in destabilization of the cliff and are important in the understanding of seacliff evolution and processes.

Along Depot Hill areas of unstable cliff occur in three distinct groups shown as areas A, B, and C on figure 6. Figure 7a shows the locations of cliff failures along an enlargement of area A. In this area, slope failures occurred along approximately 125 m of cliff and were recorded during each documented time period. The failures are localized; certain portions of the cliff appear to be stable over the short-term period from October 1989 to March 1998. A major blockfall, shown by the debris on the beach in the 1989 imagery, occurred during the Loma Prieta earthquake. This blockfall is shown by the westernmost orange line in figure 7a. Additional slope failures occurred at this same location over the decade from October 1989 to January 1998 (red lines) and resulted in further landward retreat of the cliff edge. During winter 1998 storms, seacliff failures were observed in both February (blue lines) and March (green lines) on figure 7a. These later storm-related slope failures were identified from the rectified photographic stereo models as debris flows involving only the upper terrace deposits and did not involve failure of the primary cliff-forming unit (Purisima Formation).

The second group of active cliff failures along Depot Hill is shown in figure 7b as an enlargement of area B in figure 6. As in area A, most failures in this central area recur in the same place as, or immediately adjacent to, previous failures. In area B, cliff failures over the decade and during the early 1997-98 El NiÒo storms resulted in some cliff retreat (red and blue lines in figure 7b). No failures were documented in area B for the final time period from February 1998 to March 1998, a time of moderate storm activity.

The easternmost of the areas of slope failure is shown in Figure 7c, which is an enlargement of area C in Figure 6. Based on the extent and frequency of seacliff failure, this area is the most active segment of Depot Hill during the last decade. Cliff failures occurred along approximately 145 m from October 1989 to March 1998. The failures resulted in the retreat of the cliff edge by as much as 9 m. Significant earthquake-induced failure resulted in the deposition of extensive coalescing debris fans at the base of the cliff, and a major blockfall occurred during the period from January to February 1998. This blockfall resulted in the largest single cliff retreat (9 m) measured along Depot Hill during the period of the study. The failure of this large block of the Purisima Formation resulted in a morphologic smoothing of the cliff section by removing a promontory. This promontory was flanked on both sides by normal faults, and the local morphology appears to be influenced by fault locations to some degree, with the faults typically occurring at the edges of the recesses and promontories.

The linear extents of cliff failure represented by the colored lines in figures 7a, b, and c show that the distribution of slope failures along Depot Hill is grouped, with gaps between failures of 200 to 300 m where the cliff has been virtually inactive over the period of the study. The grouping of failures indicates a spatial relationship of recurring slope failures that may be related to weakening of the cliff material from intense seismic shaking during the Loma Prieta earthquake. Faults do not appear to be a primary control on the areas of failure; they exist as frequently in the unstable areas as in the stable areas. With the exception of the large blockfall in area C, the failures are not, at a decadal time scale, leading to an overall morphologic straightening of the Depot Hill section of cliff; most of the failures are within embayments, acting to exaggerate the shore parallel cuspate morphology. The longest stretch of stable cliff occurs in the central portion of Depot Hill. The elevation in this central area is lower (17 m) than the average of 28-30 m suggesting that the cliff may be more stable where it is lower in height.

Aerial photograph from Coastal Aerial Mapping System (CAMS), March 6, 1998

Universal Transverse Mercator projection, zone 10

Figure 7a. Enlarged section of the western end of orthophotomosaic (fig. 6, A) showing locations of cliff failures for four time periods.

Aerial photograph from Coastal Aerial Mapping System (CAMS), March 6, 1998

Universal Transverse Mercator projection, zone 10

Figure 7b. Enlarged section of the central part of orthophotomosaic (fig. 6, B) showing locations of cliff failures for four time periods.

Aerial photograph from Coastal Aerial Mapping System (CAMS), March 6, 1998

Universal Transverse Mercator projection, zone 10

Figure 7c. Enlarged section of the eastern end of orthophotomosaic (fig. 6, C) showing locations of cliff failures for four time periods.

Table 1. Linear extent of cliff section experiencing slope failure for each of the time periods investigated. The data is further subdivided to show the type of slope failure for each occurrence, as well as the geologic units involved, if distinguishable.

Time Interval	Debris falls (m)	Block falls (m)	Debris flows (m)	Mixed fall block and debris (m)	Block fall and debris flow (m)	Other* (m)	Total along-cliff failure per time interval
0 (instantaneous)	124.6 / Qmt and Tp** ; 79.9 / Qmt**	9.7	0	49.9 / Qmt and Tp**	0	0	264.1
8.27 yrs (October 1989 - January 1998)	0	0	23.5 / Qmt**	0	101.8 / Qmt and Tp**	66.1	191.4
0.03 yrs (January 1998 - Februrary 1998)	0	26.9 / Tp**	31.9 / Qmt**	0	25.3 / Qmt and Tp**	0	84.1
0.07 yrs (February 1998 - March 1998)	0	0	79.4 / Qmt**	0	0	0	79.4
Total along-cliff failure per failure type	204.5	36.6	134.8	49.9	127.1	66.1	

* Other, failures where type of failure could not be determined
** Qmt, terrace deposit; Tp, Purisima Formation

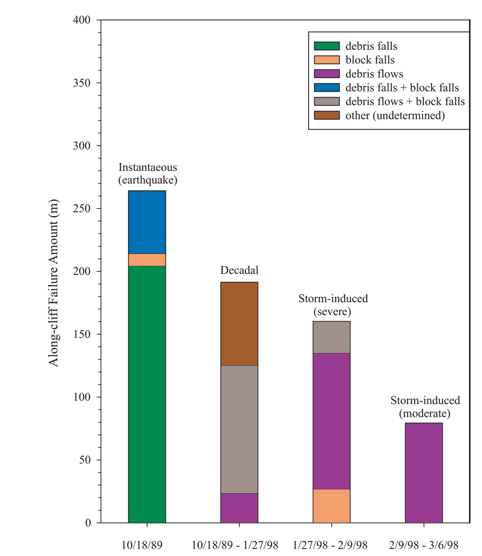

Figure 8a. Depot Hill cliff failure types, October 1989 - March 1998

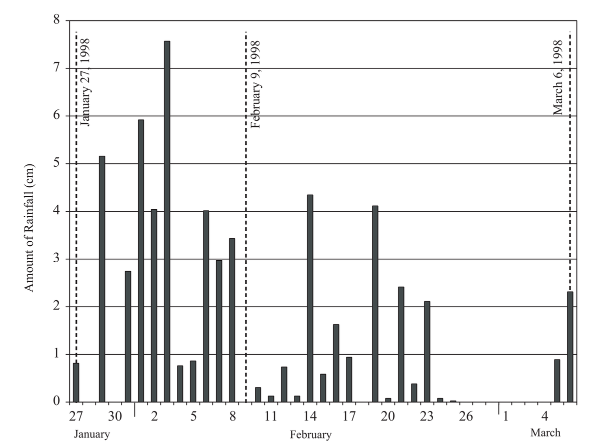

Figure 8b. Rainfall for Santa Cruz from January 27 to March 6, 1998. Dashed lines show dates of CAMS photography. Note that the period from January 27 to February 9 represents a period of high rainfall associated with severe storms, whereas the period from February 9 to March 6 was a more moderate storm period.

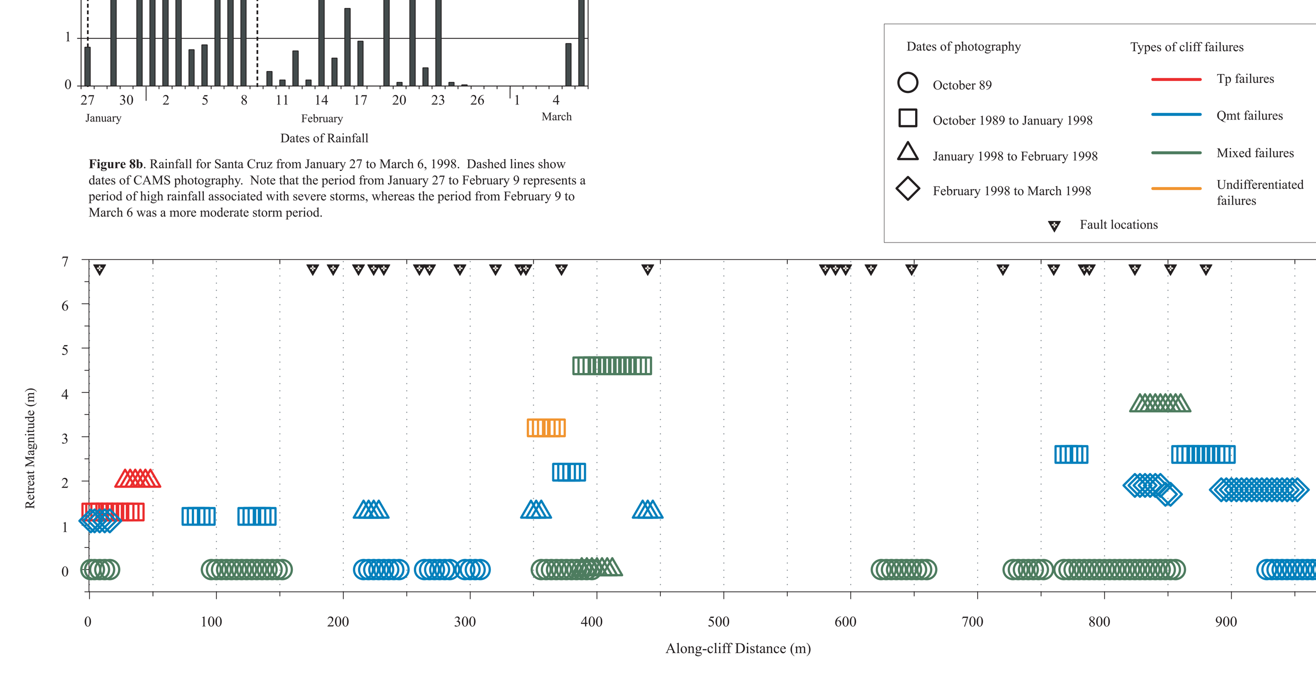

Figure 9. Plot of cliff retreat magnitudes for individual dates of photography versus the along-cliff distribution of cliff failures. The color coding shows which cliff-forming materials were involved in an individual failure, and the locations of the faults are shown at the top of the graph. In the case of the area near the beginning of the section (between 0 m and 50 m), cliff failure was identifed in the October 1989 photography as failure involving a mixture of the Purisima Formation and the terrace deposits. This is represented by the green circles. Note that all "retreat" values for the October 1989 date of photography are shown as zero. This date was used as the baseline data, and thus no other data set currently exists against which to determine the amount of retreat for this date. However, along-cliff failures are identified by deposits on the beach and scars on the cliff slope. The along-cliff distance is longer than the baseline shown in figure 6 because the baseline is a straight line approximating the average trend of this section of coast and figure 9 is showing the actual along-cliff distance.

RESULTS

Figures 8 and 9 and Table 1 summarize the overall failure styles, retreat amounts, slope failure distribution, and rainfall amounts along Depot Hill. In figure 8a, the failure types are shown in relation to the time of occurrence and the amount of the section that failed, and Table 1 shows the total amount of cliff failure for each time interval as well as the failure types. Table 1 also includes the geologic unit that failed, if this was distinguishable on the aerial photography. The category labeled "other" is in general associated with decadal slope failures wherein cliff retreat was documented but the failure style could not be discerned.

Three different types of slope failure were documented during the period from October 18, 1989 to March 6, 1998. These include debris falls, block falls, and debris flows. Rapid, seismically-induced failures were either debris or block falls, resulting in failure of 264 m of the 1 km-long cliff section. Weakening of the cliff-forming unit (Purisima Formation) as a result of seismic shaking may have contributed to the failure of the cliffs in the decade following the Loma Prieta earthquake, in which 191 m of cliff experienced mass movement. In some areas, the process of failure could not be identified due to lack of a geomorphic scar or a characteristic toe deposit. These areas were identified by a retreat of the cliff edge, and are included as "other" in Table 1, whereby the cliff retreated but the process was not observable. The period of El NiÒo storms from January 27 to February 9, 1998 (see fig. 8b) had a large impact on this section of coast. Over 160 m of cliff failed during this two-week period, predominantly as debris flows involving fluidized terrace deposits, although blockfalls involving the Purisima Formation also occurred. During the last several weeks of the El NiÒo storm period, precipitation amounts dropped and storm intensities decreased (fig. 8b). The response of the seacliffs during this time was minor; failures were documented along 79 m of the section. Small, reactivated debris flows within the terrace deposits were the only type of failure during this period.

Figure 9 is a plot of the distribution and amount of cliff failure along Depot Hill. The along-cliff distance is longer than the baseline shown in figure 6 because the baseline is a straight line approximating the average trend of this section of coast and figure 9 is showing the actual along-cliff distance. All failures documented from the October 1989 photographic stereo models are shown as having zero retreat amounts. The amount of landward retreat of the cliff edge is not available for the October 1989 date in figure 9 because the cliff position delineated from this date of photography was used as the initial position against which to measure subsequent retreat. Failure types can be recognized by geomorphic scars or toe deposits, but retreat amounts cannot be documented. Near the beginning of the section (between 0 m and 50 m), cliff failure was identified in the October 1989 photography and involved failures of both the Purisima Formation and the overlying terrace deposits (green circles). In figure 9, data from the bar graph on figure 6 and the failure locations on figure 7 are summarized. Figure 9 demonstrates the grouping of the failures in three distinct along-cliff zones; from 0-160 m, from 210-450 m, and 720-1000 m. The amounts of retreat on figure 9 are for each individual time period, whereas those shown on the bar graph in figure 6 are cumulative. The amounts of retreat vary, with the least amount of retreat occurring during the last month of the 1997-98 El NiÒo (March-98 failures), and the greatest individual failure occurring over the decade from 1989 to 1998, at approximately 400 m along the cliff. Most of the failures were either only in the terrace deposits (blue) or involved the entire cliff section of both the terrace deposits and the Purisima Formation (green).

This map has introduced new techniques of analyzing the short-term evolution of seacliffs and the differential response of seacliffs to seismic and climatic events. Using stereo models derived from softcopy photogrammetry, we are able to locate seacliff failures to determine their spatial distribution and the geologic units involved for several different time periods in an area where seacliff failure and retreat periodically threaten homes and community infrastructures. These data can be incorporated into a GIS database to examine the relationship of the failures to one another, to coastline morphology, and to field data (faults, joints, or lithologic variations). Spatial plots of the failures appear to show specific pattern; this may help in identifying areas prone to future failures and may help to understand specific processes of cliff failure and retreat. Failure of a cliff section during an earthquake may be localized where wave notching occurs at the base. This is supported by our data that shows the cliff section that is subjected to regular wave attack (Depot Hill) was more greatly impacted by the Loma Prieta earthquake than by the 1997-98 El NiÒo and the decade in between. In the short term (weeks to a decade) when there is not sufficient time to re-cut notches, the cliffs fail in response to high rainfall events.

REFERENCES

Anders, F.J., and Byrnes, M.R., 1991, Accuracy of shoreline change rates as determined from maps and aerial photographs: Shore and Beach, v. 59, no. 1, p. 17-26.
Brabb, E.E., 1989, Geologic map of Santa Cruz County, California: U.S. Geological Survey Miscellaneous Investigation Series Map I-1905, scale 1:62500.
Dupre, W.R., 1975, Maps showing geology and liquefaction potential of Quaternary deposits in Santa Cruz County, California, U.S.: U.S. Geological Survey Miscellaneous Field Studies Map MF-648, scale 1:62500.
Greene, H.G., 1977, Geology of the Monterey Bay region: U.S. Geological Survey Open-File Report 77-718, 347 pp.
Griggs, G.B., 1994, California's Coastal Hazards: Journal of Coastal Research Special Issue No. 12, p.1-15.
Griggs, G.B., and Johnson, R.E., 1979, Coastal Erosion, Santa Cruz County: California Geology, v. 32, no. 4, p. 67-76.
Griggs, G.B., and Johnson, R.E., 1983, Impact of 1983 Storms on the coastline of Northern Monterey Bay, Santa Cruz County: California Geology, v. 36, no. 8, p.163-174.
Griggs, G.B., and Savoy, L., eds., 1985, Living with the California coast. Durham, North Carolina, Duke University Press, 393 p.
Griggs, G.B, and Scholar, D.C., 1998, Coastal erosion caused by earthquake-induced slope failures: Shore and Beach, v. 65, no. 4, p. 2-7.
Hapke, C.J., and Richmond, B.M., 1999, The development of a coastal aerial mapping system (CAMS) and its application to the study of coastal morphodynamics: Coastal Sediments '99, v. 3, p. 2398-2413.
Hapke, C.J., and Richmond, B.M., 2000, Monitoring beach morphology changes using small-format aerial photography and digital softcopy photogrammetry: Environmental Geosciences Special Issue on Coastal Hazard Mapping Techniques, v. 7, no. 1, p. 32-37.
Kuhn, G.G., and Shepard, F.P., 1979, Accelerated beach-cliff erosion related to unusual storms in southern California: California Geology, v. 32, no. 3, p. 58-59.
Maher, Norman, and Wong, F.L., 2001, Low-resolution (250-m) gridded bathymetry and shaded relief image (CCALBATG, CCALSHD.TIF) of the region offshore of central California between Point Reyes and San Simeon, *in* Wong, F.L., and Eittreim, S.E., 2001, Continental Shelf GIS for the Monterey Bay National Marine Sanctuary: U.S. Geological Survey Open-File Report 01-179.
Moore, L.J., Benumof, B.E., and Griggs, G.B, 1999, Coastal Erosion Hazards in Santa Cruz and San Diego Counties, California: Coastal Erosion Mapping and Management, Journal of Coastal Research Special Issue No. 28, p. 121-139.
Plant, N.G., and Griggs, G.B., 1990, Coastal landslides caused by the October 17, 1989 earthquake, Santa Cruz County, California: California Geology, v. 43, no. 3, p.75-84.
Storlazzi, C., and Griggs, G.B., 2000, The influence of El NiÒo-Southern Oscillation (ENSO) events on the evolution of central California's shoreline: Geological Society of America Bulletin, v. 112, no. 2, p. 236-249.
Sydnor, R.H., Griggs, G.B., Weber, G.E., McCarthy, R.J., and Plant, N.G., 1990, Coastal bluff landslides in Santa Cruz County resulting from the Loma Prieta earthquake of 17 October, 1989: The Loma Prieta (Santa Cruz Mountains, California) earthquake of 17 October 1989: California Department of Conservation, Division of Mines and Geology, Special Publication 104, p. 67-82.
Thieler, E.R., and Danforth, W.W., 1994, Historical shoreline mapping (II): Application of the digital shoreline mapping and analysis system (DSMS/DSAS) to shoreline change mapping in Puerto Rico: Journal of Coastal Research, v. 10, no. 3, p. 600-620.
U.S. Army Corps of Engineers, 1985, Geologic framework report, Monterey Bay, coast of California storm and tidal waves study, Ref. No. CCSTWS 85-2.
Varnes, D.J., 1958, Landslide types and processes: Highway Research Board Special Report 29, p. 20-27.

MAP SHOWING SEACLIFF RESPONSE TO CLIMATIC AND SEISMIC EVENTS, DEPOT HILL, SANTA CRUZ COUNTY, CALIFORNIA

By
Cheryl J. Hapke, Bruce M. Richmond, and Mimi M. D'Iorio

2002

Manuscript approved for publication June 10, 2002

This map was printed on an electronic plotter directly from digital files. Dimensional calibration may vary between electronic plotters and between X and Y directions on the same plotter, and paper may change size due to atmospheric conditions; therefore, scale and proportions may not be true on plots of this map.

For sale by U.S. Geological Survey, Information Services, Box 25286, Federal Center, Denver, CA 80225, 1-888-ASK-USGS

Available on the World Wide Web at http://geopubs.wr.usgs.gov/data.html